ZenseTag: An RFID assisted Twin-Tag Single Antenna COTS Sensor Interface

Nagarjun Bhat, Agrim Gupta, Ishan Bansal, Harine Govindarajan, Dinesh Bharadia
University of California San Diego
La Jolla, United States
{nbhat,agg003,isbansal,hgovindarajan,dbharadia}@ucsd.edu

Abstract

Sensors enable us to digitally capture stimuli like moisture, light, and force. Despite their low cost, reliability, and scalability, the lack of widespread adoption of IoT has hindered the realization of true ubiquitous sensing. A likely reason is that the current sensor platforms are bulky due to the batteries and complex electronics needed to interface sensors communication systems. In this work, we present a fully-passive, miniaturized, flexible form factor sensor interface titled ZenseTag that uses minimal electronics to read and communicate analog sensor data, directly at radio frequencies (RF). We exploit the fundamental principle of resonance, where a sensor's terminal impedance becomes most sensitive to the measured stimulus at its resonant frequency. This enables ZenseTag to read out the sensor variation using only energy harvested from wireless signals. We demonstrate its implementation with a 15x10mm flexible PCB that connects sensors to a printed antenna and passive RFID ICs, enabling near real-time readout through a performant GUI-enabled software.

We showcase ZenseTag's versatility by interfacing commercial **force**, **soil moisture** and **photodiode** sensors [1–3]. Further, we motivate dedicated application studies for these sensors.

CCS Concepts

• **Hardware** → *Emerging technologies*; **Circuit substrates**; **Sensors and actuators**; **Sensor devices and platforms**; **Wireless devices**; **Sensor applications and deployments**;

ACM Reference Format:

Nagarjun Bhat, Agrim Gupta, Ishan Bansal, Harine Govindarajan, Dinesh Bharadia. 2024. ZenseTag: An RFID assisted Twin-Tag Single Antenna COTS Sensor Interface. In *ACM Conference on Embedded Networked Sensor Systems (SenSys '24), November 4–7, 2024, Hangzhou, China.* ACM, New York, NY, USA, 15 pages. https://doi.org/10.1145/3666025.3699342

1 Introduction

Sensing technologies are crucial for perceiving and actuating our environment by converting various stimuli, such as light, force, and humidity, into digital values. For example a farmer can automate irrigation if sensors can monitor soil-moisture as shown in Fig. 1a, or an athlete can monitor performance and recovery by measuring ground-reaction-forces while running as shown in Fig. 1b. Recently, they have expanded to measure a wide range of stimuli, including forces[4], oral health [5], chemical/biological phenomena [6–9], with growing adoption in applications like user interaction, health monitoring, and contaminant detection. As novel sensors evolve, they move us closer to the grand vision of ubiquitous sensing [10]: sensors embedded into everyday life, enabling continuous, real-time data collection across diverse domains making systems more adaptive to human needs with minimal intervention.

However, advancements in sensor capabilities alone are insufficient to achieve this vision; we need other the components of sensing such as, sensor interfaces and communication systems to evolve in parallel. Unfortunately, these components have not progressed at the same pace, and has hindered the widespread adoption of these sensors. Consider the digital sensor interfaces that use low-power microcontrollers (MCUs) to digitize sensor outputs and communicate via BLE, LoRa, or ZigBee [11–13]. These solutions still rely on bulky circuits and ADCs that consume several mWs of power[14], necessitating the use of batteries to meet power budget. This limits their use in widely-touted innovative biomedical applications, like "smart-shoes" that can measure foot-impact forces during athletic activity [15–19]. Even when form factor isn't a concern, as illustrated in Fig. 1a , batteries present significant environmental risks, especially as these sensors become more widespread [20–22]. This reliance on batteries contradicts the deploy-and-forget paradigm that enhances the appeal of IoT.

Alternatively, analog sensing platforms directly modulate wireless signals such as Wi-Fi [23, 24] / BLE [25] and LoRA [26] using sensor outputs, bypassing digitization. However, many of these methods face challenges such as unreliable sensor readout, poor latency and the need for costly hardware modifications. Furthermore, they rely on customized sensors and do not generalize well to COTS sensors, and often require bulky energy harvesting or interface electronics/PCBs and do not lend themselves well to compact battery-free passive tags [27]. In summary, both current digital and analog sensing methodologies fall short of delivering the promise of ubiquitous sensing. In order to overcome these challenges, we need a sensing platform that uses minimal electronics, can interface with existing COTS sensors, is robust to multipath, can be scaled inexpensively in the form of miniature, flexible tags, operates passively and can be integrated into existing communication infrastructure.

One potential radio technology that satisfies the above criteria is RFID, which uses identity-carrying tags that are small, paper-like, flexible, and can be read wirelessly using even small form factor readers [28–30]. However, commercially sold RFID stickers are limited in functionality, as they can only transmit their digital identity and lack the capability to read or communicate sensor outputs that change in response to sensed stimuli. This makes the interface of commercial sensors with RFID stickers a non-trivial

SenSys '24, November 4–7, 2024, Hangzhou, China

ACM ISBN 979-8-4007-0697-4/24/11.
https://doi.org/10.1145/3666025.3699342

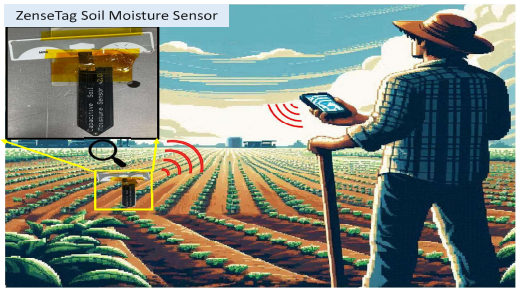

(a) Battery-free Soil moisture sensing in Farms (AI-generated image)

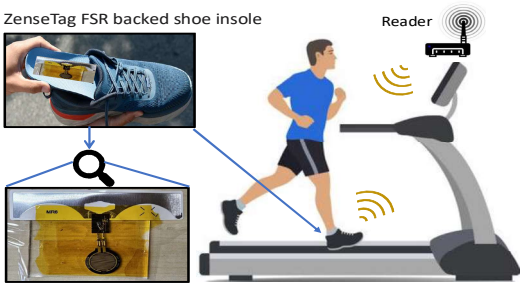

(b) Battery-free wearable shoe-insole based force sensing.

Figure 1: Enabling ubiquitous applications of battery-free sensing

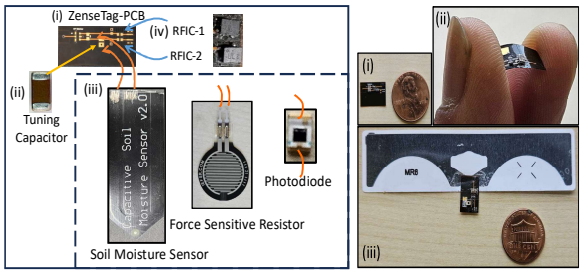

(a) Sensor interface PCB of ZenseTag (b) ZenseTag with sensor

Figure 2: Versatile sensing with ZenseTag.(a): (i) ZenseTag PCB to interface with sensors. (ii) Tuning capacitor to move resonance; (iii) Various sensors interfaced with our platform; (iv) RFID ICs that are used in ZenseTag (b): (i), (ii) Small and flexible form factor of ZenseTag; (iii) PCB attached to a COTS RFID antenna.

challenge. Although past works show how RFID can be used to read forces, temperature, moisture and touch interaction [4, 31–34] using dedicated and novel sensors for RFID integration, their performance degrades severely when commercial off the shelf (COTS) sensors are used instead [35]. Additionally, in the absence of a digitization mechanism, the sensor readouts modulated atop RFID signals are highly susceptible to corruption by multipath effects [31, 32, 36], posing a serious reliability problem. In our work, titled ZenseTag, we develop a novel RFID-assisted sensing platform that interfaces COTS sensors (Fig. 2) to inexpensive, flexible RFID stickers.

We outline the following core contributions of ZenseTag:

- **Improved Analog readout for COTS sensors**: We methodically profile the impedance of commercial 2-terminal COTS sensors at RF (902-928 MHz used by RFID systems), accounting for parasitic effects to enable **Direct-to-RF Interfacing of COTS Sensors**. Furthermore this interfacing technique can be extended to any other RF wireless technology. More importantly, ZenseTag utilizes the novel concept of impedance-resonance effect exhibited by two-terminal commercial sensors modeled as R-L-C circuits at particular frequencies where they maximally couple the stimulus to the backscatter signal. We demonstrate for the first time, how generic sensors that were hitherto posed as a challenge to work with at RF [35] can be made responsive at the appropriate frequencies using simple passive components.
- **Generality of Sensing**: We demonstrated that ZenseTag works with three commercial sensors, enabling various applications. This technique can also be applied to any sensor with terminal impedance variation.
- **Robust analog sensing with a Miniaturized, Flexible, COTS compatible PCB**: ZenseTag interfaces the frequency tuned sensor with two RFID tags using a **Twin-Tag Single-Antenna Sensor Interface**, such that one tag is modulated with the sensor stimuli, while other is isolated. This is done with just a 15mm x 10mm flexible PCB that connects these three components: sensor and the two RFID tags, to a single printed RFID antenna. The RFID reader then decodes the analog sensor data by comparing the relative channel measurements from the two tags.
- **Low-latency RFID reader software**: We read the tags using a COTS RFID reader (Impinj Speedway) and an open-source library, SLLURP [37] that can be implemented on any general purpose computing platform. Using a PyQT-designed GUI, we show near real-time sensor readout, as highlighted in our demo videos for **force**, **soil moisture** and **light intensity** sensing [1–3].
- **Power Consumption**: We highlight that the ZenseTag platform consumes no power beyond what the RFID tags use, operating solely on RF harvesting from a reader without needing additional energy sources.

We evaluate the merits of ZenseTag by interfacing it with multiple COTS sensors such as a Capacitive Soil Moisture sensor [38], a Force Sensitive Resistor (FSR) [39], and a Photodiode [40]. Using real-world case studies, we summarize the following performance metrics for our platform :

- We achieve **>93% accuracy** for 3-level soil moisture classification (**Dry/Moist/Saturated**) and estimate moisture in an outdoor soil bed using three separate sensors [2].
- ZenseTag accurately measured loads as small as 10g (0.1N) and was used to implement a real-time human stepping force sensor, demonstrating low-latency operation [1].
- We demonstrate **over 85% accuracy** in classifying three distinct brightness levels with a commercial photodiode and showcase a passive, real-time binary light-intensity detector using ZenseTag [3]. Additionally, we built a fully passive wavelength classifier that can distinguish between Red, Yellow, and Blue light.
- ZenseTag achieved a median phase error $< 4^\circ$ degrees, representing a **8X** improvement over previous dual RFID tag approaches ($> 30^\circ$) [32] in terms of resilience to multipath-induced phase errors.

- Finally, ZenseTag accomplishes the above using an ultra miniaturized, flexible PCB measuring just $\mathbf{150}mm^2$ as shown in Fig. 2.

2 Related Work

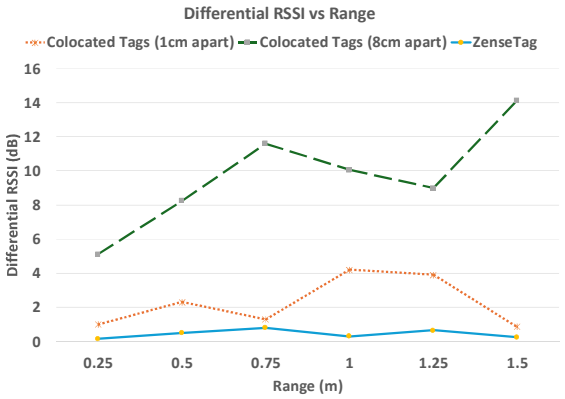

Figure 3: Prior approaches with colocated dual tags show significant RSSI variation, even at 1 cm apart due to coupling, worsening with separation distance. In contrast, ZenseTag maintains a differential RSSI of <0.5 dB, unaffected by reader-tag distance.

Given the myriad of applications and pervasive deployments enabled by batteryless and wireless sensors, there has been multiple related research attempts to ZenseTag. But unlike, ZenseTag, the past approach fails to interface multiple commercial sensors (like force, soil moisture and photodiode) with easily available and cheap RFID stickers. Further, ZenseTag interface also allows simple software built atop standard RFID readers to also read the sensor data in addition to the typical RFID decoding. This section summarizes these related works, and puts ZenseTag's contributions in context with the past explorations.

Digital Sensor Interfaces with RFID Systems: The past works in this category harvest RF energy to power up extremely low-power electronics (ADCs, microcontrollers) that can both digitize and communicate sensor data to a remotely located RFID reader [11, 12, 41–45] However, there is a fundamental limit to these approaches, since beyond a point the ADC/microcontroller power consumption can not be reduced further [13], and hence, most of these approaches still require more energy to power up than what is supported by existing energy harvesters. As a consequence, these approaches use bulkier antennas instead of printed flexible antennas, or larger capacitors to support the higher energy requirement, and are difficult to miniaturize [11, 12, 46]. Hence, even though these approaches adopt the same RFID protocol (EPC) and add digital sensor data transmission over it, the actual prototypes are larger than the typical RFID stickers. An added problem is also that of increased latency, these approaches need to collect energy for a larger amount of time to be able to communicate, which makes the sensor readout more intermittent. ZenseTag side-steps this problem by not requiring the dedicated electronics to digitize the sensor data, and instead communicates the sensor data in the analog domain.

Analog Sensor Interface with RFID Systems: Communicating sensor data in analog domain reduces the energy constraints imposed by the digital counterparts. However, so far, analog sensor interfaces have been demonstrated for dedicated sensor stimuli, for example, contact forces [4], photo-diodes [47], temperature sensors [33, 48], or touch-based interaction sensors [34, 49–51]. These approaches are not designed to sense multiple types of stimuli on the same platform and are optimized for specific stimuli only. Further, the shown sensor stimuli in these past work require a new dedicated sensor design that is not COTS, which limits their adoption. It also has been shown that interfacing commercial sensors with RFID stickers leads to reduced performance [35], with a drastic loss in sensor readout accuracy. In ZenseTag, we show methods that can allow interfacing commercial sensors in analog domain with RFID stickers to a sufficient degree of accuracy. This is achieved by carefully profiling the sensor impedance and matching it appropriately to RFID impedance to enable a maximal coupling between the RFID and sensor stimuli. Additionally, ZenseTag performs low latency sensor readout compared to lengthy estimation times [35, 52].

RFID tags as a sensor: Given the difficulties in interfacing external sensors, some prior works explore using an RFID tag itself as a sensor. Herein, the goal is to isolate the RFID channel variations caused by different stimuli (like moisture, temperature, dielectric), due to the coupling between the RFID antenna and environment [31, 32, 36, 53, 54]. Even though some of these approaches use multiple RFID tags, with a few tags exposed to stimuli and others don't, in order to isolate the changes due to a particular stimuli [31, 36, 52, 55], these approaches are not scalable. Also, these approaches are not able to isolate one sensor stimuli from the other, for example, a moisture changing RFID channel can also change from temperature effects. ZenseTag's capability to interface dedicated analog sensors provides a way of generalizing these approaches to multiple environments, and as well provide sensor stimuli isolation. That is, these approaches can not generalize across multiple environments, that can create different coupling effects. Furthermore, prior RFID-based sensing solutions often use a dual-tag approach, where tags are placed in close proximity ($< \lambda/2$) to mitigate multipath effects in dynamic environments. However, this method tends to suffer from poor readout accuracy due to signal inconsistencies between the antennas or strong coupling when they are positioned too closely. As demonstrated in Fig. 3, and Sec. 5, the differential RSSI comparison between the two methods clearly shows improved reliability when using a single antenna as in ZenseTag, despite a loss in range due to loss from the Wilkinson power divider.

Non-RFID platforms: Finally, some recent analog sensor interfaces use non RFID platforms such as audio, LoRA, WiFi and light to communicate sensor data [23, 49, 56–59]. However, unlike the RFID platforms, these approaches use bulky rigid PCBs [23, 49, 60, 61] with multiple discrete electronics, and additional energy harvesters that only work in well-lit environments or or do not account for the energy consumed by the sensor interface itself [23]. Additionally, some backscatter approaches that use JFETs as voltage-impedance transformers or frequency modulators [49, 62, 63], use USRP based implementation and are incompatible with commercial RFID readers. Moreover, these systems are optimized for specific operating conditions to achieve low-power sensing and do not generalize well to COTS sensors, which often introduce parasitics that disrupt the fine-tuned setup and deteriorate the accuracy of sensing [49]. In contrast ZenseTag achieves >90% accuracy for all three COTS sensors Further, as a consequence of being early stage prototypes,

these platforms require SDRs which requires dedicated software to be written for real-time demos and latency optimization. On the other hand, RFID platforms have had decades of research backing the development of sticker-like tags, which are readable with commercially available RFID readers. Thus ZenseTag offers a sensor platform compatible with affordable RFID stickers and software for low-latency sensor readout using commercial RFID readers.

3 Design

In the following section, we will go over the design steps of ZenseTag, and explain how ZenseTag is able to interface different COTS sensors (force, soil moisture and photodiode [1–3]) with easily available RFID stickers. The key to interface commercially available sensors with RFID stickers lies in performing 'Direct-to-RF' Impedance profiling, which models sensor behaviour directly at Ultra High Frequency (UHF). Next, using this model, ZenseTag makes a vital discovery: most of the commercial sensors exhibit a resonant frequency effect, at which they become very sensitive to the particular stimuli. Furthermore, akin to the resonant frequency tuning of antennas, the sensors' resonant frequency can be tuned to match that of RFID tags. Additionally, ZenseTag creates a novel 'Twin-Tag Single-Antenna Sensor Interface' using flexible PCBs, which allows interfacing of the frequency tuned sensor to twin-RFID ICs, both interfaced to a single antenna to minimize the form-factor. The flexible PCB ensures that one IC is coupled with the sensor stimuli, whereas the other is isolated. Finally, a commercial RFID reader reads the two ICs, and computes their channel difference to demodulate the sensor impedance, thus creating a low-latency sensor readout, which is robust to even dynamic environments. Hence, ZenseTag's design can be summarized to three contributions: (1) Direct-to-RF Impedance profiling, which models sensor behaviour directly at RF and can directly modulate the backscatter signal. (2) Leveraging the impedance resonance of COTS sensors and tuning it to improve their readability at RF. (3) Twin-Tag Single Antenna Sensor Interface enables robust sensor impedance readout by matching the sensor to two tags and an antenna., and (4) Low-latency sensor readout via software developed atop a commercial RFID reader.

3.1 Direct to RF Interface: Modelling commercial sensors at RF frequencies

Many commercial sensors react to changes in the measured stimulus by altering the voltage or current across their interfacing terminals. This variation can be modeled as a change in terminal impedance, which can then be used to modulate one or more parameters of a wireless signal directly at RF (which we call direct-to-RF interface). Most of the prior-work treats sensors as pure capacitors [4, 23, 49], or pure resistors [32, 58, 64]. This is true only at low-frequencies (LF) [49], or when sensors have a parallel plate structure which guarantees capacitive behaviour even at RF [4, 65]. However, when the commercial sensors are interfaced directly to RF, they exhibit complex impedance as shown in Eq. 1, where X_{sensor} represents the reactive component of the impedance, wherein $X_{\text{sensor}} > 0$ if the sensor impedance is inductive and $X_{\text{sensor}} < 0$ if capacitive.

$$Z_{\text{sensor}} = R_{\text{sensor}} + j * X_{\text{sensor}} \tag{1}$$

Furthermore, X_{sensor} is a function of frequency and can vary vastly. For example, a soil moisture sensor that is capacitive at kHz frequencies may behave as an inductor at some MHz frequencies and may even develop a resistance profile. Our measurements, of a soil moisture 'capacitor' and a force-sensitive 'resistor' (Fig. 4), show that sensor impedance behavior differs significantly between DC (or LF) and RF. The reason for this deviation from the expected behaviour at RF frequencies, is the complex construction of sensors. For example, a force-sensitive resistor has an inter-digitated structure, which can act as inductor coils at certain frequencies, whereas a soil-moisture capacitor has long, and lossy resistive leads. These complex impedance behaviors are difficult to quantify without electromagnetic simulations of their actual physical models. Consequently, it is challenging to account for them when developing a direct-to-RF sensor interface. In ZenseTag, we demonstrate a methodical procedure to profile the impedance of any commercial sensor. The key insight we have to handle these non-idealities, is to treat the sensors similar to RF antennas. Sensors act as transducers and couple a particular stimulus to a measurable change in an output parameter such as impedance. This is similar to the behavior of antennas that in-fact act as transducers of electromagnetic energy. Thus, at a fundamental level, the transduction principle of both sensors and antennas are similar.

Hence, in order to directly profile the sensor impedance at RF, we can treat them as antennas, and obtain their scattering parameters (S_{11} measurement) as shown in Fig. 5. The S_{11} plot is obtained by exciting the sensor at a particular RF frequency, and observing the resultant amplitude/phase change back from the sensor. We use this S_{11} measurement to profile the impedance of the sensor, using the relationship shown in Eq. 2. The sensor impedance profile reveals several crucial details that guide our design and implementation: Depending on the sensor impedance profile and the parameter that varies as a function of stimulus (R_{sensor} or X_{sensor}), we can interface it in either a series or shunt configuration as in Fig. 6a. Basically if the sensor resistance is small and varies with stimulus it can be interfaced in series and in shunt if the value of a parasitic resistance is very large. On the other hand, if a sensor is reactive dominant, then it is interfaced in shunt configuration as shown in Fig. 6.

Now that we have profiled the impedance of the sensor at RF, how do we achieve direct-to-RF interface with the tags? To do that, we utilize a key insight: The complex reflection coefficient Γ that is used to obtain the impedance profile, can also be used to model the relationship between an incident signal S_{inc} and its backscatter: S_{bs}. The signal returned by the RFID IC, is given simply by Eq. 3. This relationship shows how variations in the sensor impedance Z_{sensor} in response to changes in the measured stimulus can be coupled directly at RF to the backscattered signal, thus modulating its phase and amplitude. This modulation is then decoded at the reader end.

$$\Gamma = Refl.\ Wave/Input\ Wave = \frac{Z_{sensor} - Z_0}{Z_{sensor} + Z_0} \tag{2}$$

$$S_{\text{bs}} = \Gamma * S_{inc} \tag{3}$$

3.1.1 ***Frequency Agnosticism of Direct-to-RF-Interface:*** The technique direct-to-RF sensor interface where we map changes in terminal impedance directly to carrier amplitude/ phase is universal and agnostic to the radio frequency of interest (UHF RFID in this case). Essentially, since this technique relies simply on the principle

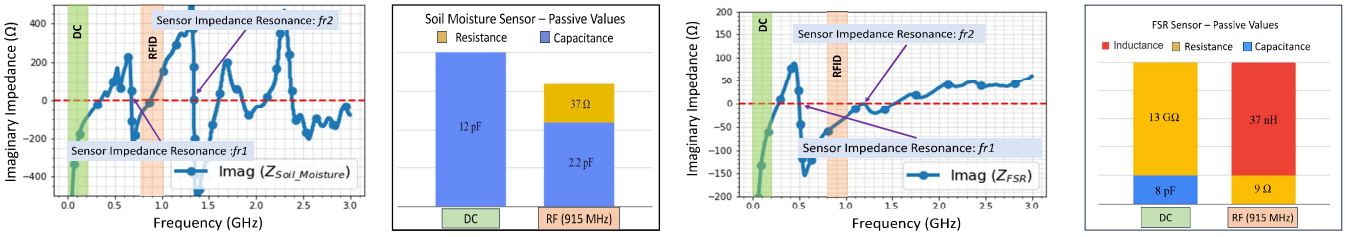

(a) (b) (c) (d)

Figure 4: Accurate impedance characterization: (a) Frequency profile of imaginary impedance of a commercial Soil Moisture Sensor. (b) Impedance comparison of soil moisture sensor measured at DC and 915MHz. (c) Frequency profile of imaginary impedance of a commercial FSR. (d) Impedance comparison of commercial FSR at DC and 915MHz

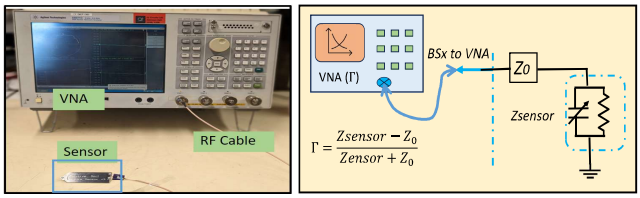

(a) VNA setup (b) Impedance profiling topology

Figure 5: Sensor Impedance profiling using VNA

of impedance modulated backscatter, it can be extended to other frequencies/wireless technologies such as LoRA, WiFi or Bluetooth. Having accurately profiled the sensor impedance, we now optimize the sensor response at the desired frequency.

3.2 Impedance-Resonance Tuning: Enhancing Sensor Readout at RFID frequency band

In ZenseTag, we communicate the analog variations in the sensor impedance over RFID backscatter signal. On their own, if interfaced directly to an analog interface, these commercial sensors might exhibit no change in terminal impedance in response to the stimulus. To address this challenge, we leverage a key insight of ZenseTag: even these sensors exhibit an enhanced impedance response at specific frequencies. Similar to antennas that are most efficient at their resonant frequencies (or fundamental modes), sensors also exhibit an enhanced impedance response at its 'resonant frequency'. Thus, at these particular frequencies, they are able to maximally couple changes in stimulus to their terminal impedance, as shown in Fig. 7a. While sensors show enhanced response at their resonant frequencies, these do not necessarily align with the carrier frequency (902-928 MHz for RFID). In other words, at these resonant frequencies the sensor responsiveness to a change in the stimulus is at its best. Hence we need to "tune" this sensor impedance-resonance to near the RFID band for maximum sensitivity and performance. Drawing on the analogy with antennas, which often require dimensional adjustments to operate within the correct frequency band, the ZenseTag sensor interface similarly requires fine-tuning to ensure that the sensors function at the desired frequency band.

To show how we can make these fine adjustments in sensor resonance frequency, we consider the example of a capacitive soil moisture sensor, whose equivalent RF model is shown in the circuit Fig. 7. Although a particular capacitance value C_{fr1} is provided at DC or low-frequencies, at RF, due to packaging effects, leads etc., an additional parasitic inductance L_{par} and equivalent series resistance (ESR) are inherently present. These parasitic components L_P and C_{fr1} will resonate with each other at sensor resonance-frequency (SRF) f_{r1} and beyond that, the sensor could behave as an inductor as can be seen from the phase reversal in Fig. 7b. Keeping this in mind, the design target is to move the SRF to a value slightly outside the frequency band of interest. Since SRF f_{r2} lies very close to the RFID frequency, we will move this resonant frequency to a value f_{new} such that it falls below 900MHz. Antenna designers frequently leverage the concept of aperture tuning [66] to move the resonance frequency of antennas, enhancing their sensitivity and radiation efficiency in a desired band. Similarly, in ZenseTag, we tune the SRF of the soil moisture sensor to improve its sensitivity in the UHF RFID band, by simply adding a general tuning capacitor C_{tune} and/or inductor L_{tune} as needed. The mathematical formulation of the same is shown in equation 4. Placing the moisture sensor in soil and the addition of water moves the frequency further down to about 874MHz as shown in Fig. 7b. Although the sensor alone wasn't responsive to soil moisture changes at UHF RFID, resonance tuning improved its sensitivity.

$$f_{\text{new}} = \frac{1}{2\pi}\left(\sqrt{L_{\text{par2}} \cdot C_{\text{eff}}}\right), \quad \text{where} \quad C_{\text{eff}} = C_{\text{fr2}} \parallel C_{\text{bias}} = C_{\text{fr2}} + C_{\text{bias}} \tag{4}$$

A key advantage of ZenseTag is that its matching and tuning process is entirely passive, requiring only a single bias capacitor and no power. In contrast, previous analog sensing approaches, such as [48, 49], use oscillation circuits to transduce sensor impedance into analog frequency shifts, which requires additional energy harvesters like photodiodes. Moreover, with commercial sensors, the impedance becomes more complex. To compensate for the higher reactance, the inductors used in the oscillation circuits [48, 49] must be larger, increasing the overall size. In comparison, ZenseTag's impedance tuning just requires a single surface mountable bias capacitance that is almost the size of a rice grain.

So far we have shown how the complex impedance of COTS sensors can be analogous to antenna impedance profiling and tuning, in order for the sensors to create measurable analog phase/amplitude changes at a desired frequency band. We will now describe how to reliably read these commercial analog sensors in real-time under the influence of dynamic multipath effects.

3.3 Twin Tag Single Antenna Integration for Sensor Readout via RFID Reader

To ensure robust passive analog sensing, the analog changes (phase/amplitude) introduced by the sensor should be readable even in a cluttered environment with moving objects and people. Prior approaches have used a reference tag that is co-located with the sensor

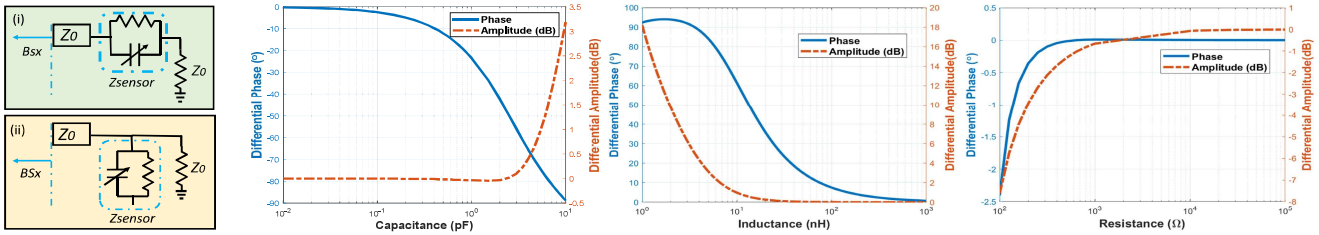

(a) (i): Series (ii): Shunt (b) Capacitive sensor in shunt topology (c) Inductive sensor in shunt topology (d) Resistive sensor in shunt topology

Figure 6: Choice of topology based on characteristic sensor impedance values. Note that the native impedance impacts differential RSSI/ phase significantly.

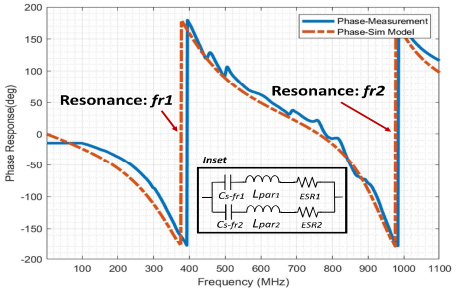

(a) Sensor's inherent impedance-resonance frequencies

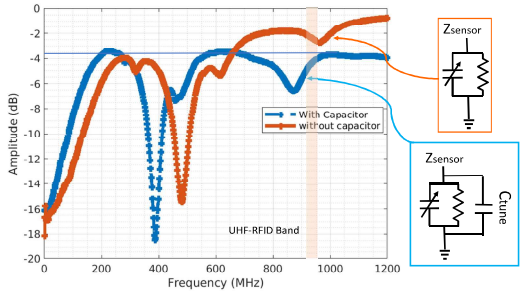

(b) Tuning the sensor impedance resonance with passive components

Figure 7: The complex sensor impedance shows a sharp response to changes in the measured stimulus near its resonant frequencies.

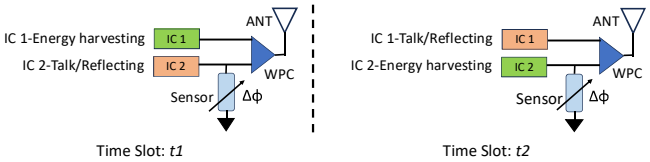

Figure 8: ZenseTag enables a Twin-Tag-Single-Antenna interface where a commercial reader communicates with the two tags at different MAC time slots.

modulated tag [31, 32, 52], assuming they both experience identical channels. However, as shown in Figs. 9b,17, the signal that travels to the two tags may travel different path lengths, thereby accruing an additional non-deterministic phase/amplitude difference that corrupts the sensor readout. A better way to solve the differential sensing problem is to use a Twin-tag Single Antenna PCB, where both the tags are connected to a single antenna, [34, 67]. However, they use bulky, rigid, patch antennas that cannot be miniaturized.

ZenseTag solves this problem using an IC version of the Wilkinson Power Combiner (WPC) as shown in Fig. 10. Basically the compact WPC ensures that the two *IC1* and *IC2* are sufficiently isolated(>25dB) from each other while the reader reads them across different time slots *t1* and *t2* [68, 69], as shown in Fig. 8. Essentially at MAC (Medium Access Control) time slot *t1*, IC1 is in energy harvesting mode while IC2 is in reflect/talk mode, responding to the reader's queries. At time slot *t2*, their modes get switched. Note that the reader reads these tags in very quick succession (read rates >1kHz), and hence the channel will not change appreciably between those time slots. While the reader is able to separate the the tags using unique EPC codes, sufficient isolation is still necessary at the hardware level to ensure that the analog phase of the carrier is not corrupted. This isolation also guarantees that the changes in sensor phase affects only one tag and the other tag is immune from it, serving as a reliable reference.

Additionally, RF simulations confirm that the Wilkinson Power Combiner (WPC) effectively isolates the sensor impedance fluctuations to the specific port it is connected to, reducing any impact on the antenna's impedance. The WPC splits an incoming signal into two equal halves at its output ports (Port 2,3 as shown in Fig. 9a) or reciprocally combines them at its Antenna connected Port 1. The signal to Tag 2 undergoes modulation by the sensor whereas the signal to Tag 1 is backscattered as is and recombined at Port 1, connected to an antenna and then radiated back to the reader, as shown in Fig. 9a. The signals from the two tags are separated by the virtue of their unique EPC at the reader. The mathematical formulation of the same is given in Eq. 5 where the phase difference $\Delta\Phi$ introduced by the sensor is isolated from the random phase added by multi-path α by virtue of the subtraction of phases of the code-separable signals in $S_{bs}(t)$. For example the phase change introduced by the sensor can be recovered as $\Delta\Phi$ given by the differential phase between the two tags or $\angle Y_{diff}(t)$. The same concept can be extended to differential amplitude as well.

$$S_{bs}(t) = s(t) * [m_1(t) * e^{-j*\Delta\Phi} + m_2(t)] * e^{-j\alpha} \quad (5)$$

$$\angle Y_{diff}(t) = \angle(S_{bs}(t) * m_1^*(t)) - \angle(S_{bs}(t) * m_2^*(t)) \quad (6)$$

3.4 Enabling Low Latency analog sensing

Finally, to enable some of the ubiquitous applications of ZenseTag envisioned in Sec. 1, we develop a performant code that runs on a host machine connected to a commercial RFID reader. This code accounts for the pseudo-random channel-hopping of the reader, and can decode the sensor phase using just a few tag-reads, thereby enabling low-latency sensing.

Now that we have individually addressed the critical challenges faced by analog sensing platforms, we will briefly summarize the steps to build an inexpensive, compact,real-time sensing platform that can interface with any two-terminal sensor in a robust and

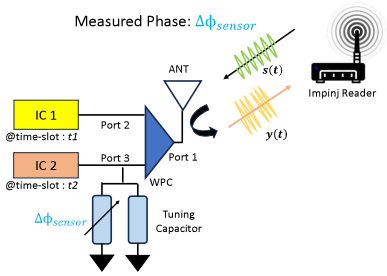

(a) Differential sensing-ZenseTag

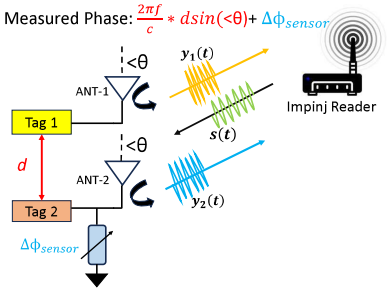

(b) Differential sensing-dual tags

Figure 9: ZenseTag uses differential analog modulation and Twin-tag-Single-Antenna interface, whereas with co-located dual tags, the phase is corrupted by the different AoA between the 2 tags.

completely battery-free manner. In ZenseTag, we design a novel Twin-Tag Single Antenna PCB that accommodates any commercial sensor without additional circuitry. It includes a tunable network to adjust sensor resonance, a Wilkinson power combiner to achieve reliable sensing and two RFID tags (sensor-modulated and reference), all interfaced with a COTS RFID antenna. Next, we implement this design on a compact, flexible PCB.

4 Implementation

In this section, we show the implementation of the ZenseTag RFID assisted sensor platform. It consists of three parts which complement the previously discussed design contribution, (1) A rigid microstrip PCB used to profile the impedance of sensors (2) A flexible PCB with RFID IC , sensor pads and surface mount component pads in the proposed π network for tuning the sensor resonant frequency and (3) A GUI implemented using the open source SLLURP library [37] to enable real-time sensor readout.

4.1 Sensor Impedance Profiling

In order to achieve Direct-to-RF interface with a commercial sensor its impedance needs to be profiled at 900MHz. Unlike DC/low frequencies (<10MHz), where LCR meters [70] or sample and hold circuits [71] are used, higher frequencies exploit a complex, frequency dependent quantity called reflection coefficient Γ. A Vector Network Analyzer (VNA) [72] is used to measure Γ which is related to the complex sensor impedance (resistive+reactive) as shown in Eq. 2). The characteristic impedance of the transmission line Z_0 is both real and known. Thus, by measuring Γ and following proper calibration and de-embedding steps [73] to eliminate fixture-induced errors, we can accurately determine the sensor's resistance and reactance. The sensor is connected to the transmission line of a rigid inexpensive FR-4 PCB as shown in Fig. 11a, and a wired measurement of Γ is recorded.

Once we derive the error-corrected sensor impedance and its resonance frequencies have been identified, we utilize Eqs. 7, 8 to decide on the topology as depicted in Fig. 10. Based on the sensor resonances, a capacitance is used to tune the sensor close to the UHF RFID band (902-928 MHz). The concept of sensor impedance profiling and resonance tuning explained here using a soil moisture sensor can be generalized to any COTS sensors.

$$\Gamma_{shunt} = \frac{Z_{sensor} - Z_0}{Z_{sensor} + Z_0} \tag{7}$$

$$\Gamma_{series} = \frac{Z_{sensor}}{Z_{sensor} + 2Z_0} \tag{8}$$

So far we have accurately profiled the sensor impedance, identified the correct sensor interface topology, and tuned its resonant frequencies using capacitors. Next, we will cover the flexible PCBs used to interface the sensor with RFID tags and connect to a COTS RFID tag antenna.

4.2 Flexible PCB for Sensor Interface

We will now review the steps involved in making the flexible PCB that gives ZenseTag its desirable properties. First, we use a commercial RF simulation tool like Advanced Design System (ADS) [74], to model the components like power divider, antenna, sensor impedance and tuning network ZenseTag at a schematic level. Following this, we design the layout in Altium, simulate the PCB and antenna using an Electromagnetics solver [75] and fabricate at a low cost (25c per PCB). The two versions of ZenseTag PCB respectively accommodate the SL3S1202 Rain RFID tag [76] and Wet-Inlay RFID tag [77] as shown in Fig. 11. We now assemble simple PCB components such as Wilkinson power combiner, 100Ω balance resistor, resonance tuning network, and finally attach a two-terminal sensor, as shown in Fig. 12. A simple 5-step procedure detailed below :

- **Step 1:** Peel the RFID in-lay tag(s) off of the COTS RFID tag carefully using forceps as shown, to expose the in-lay tag adhesive.
- **Step 2:** Solder the Wilkinson Power Combiner, and the 100Ω resistor as shown.
- **Step 3:** For the IC compatible version, the SL3S1202 RFID ICs are soldered. Similarly for the wet-inlay ZenseTag, we use forceps and the adhesive side of the inlay to stick the two ICs on the footprint provided in the flexible PCB.
- **Step 4:** The assembled PCB is now attached to the exposed pads of the flexible antenna. Once the electric contact is established, the flexible ZenseTag is ready to be interfaced with sensors.
- **Step 5:** The sensor is now soldered to the two pads provided for sensor interface and finally connect to a COTS RFID flexible tag antenna.

Once the tags have been fabricated, assembled and the sensor has been correctly tuned and interfaced with ZenseTag PCB, we can move onto set up a real-time wireless measurement using the GUI we developed.

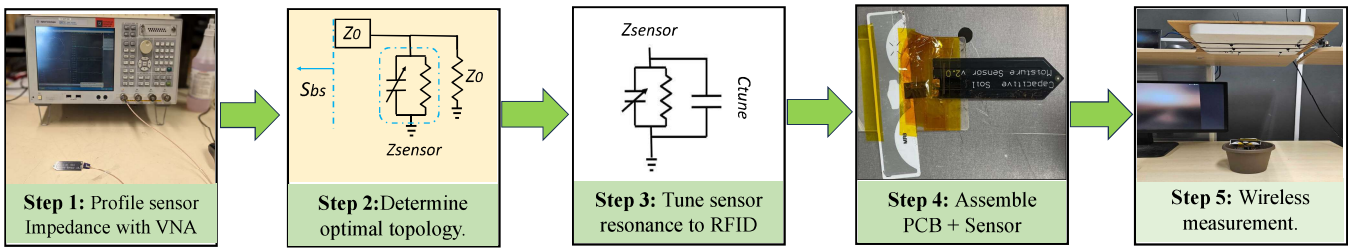

Figure 10: Step-wise Implementation workflow of ZenseTag

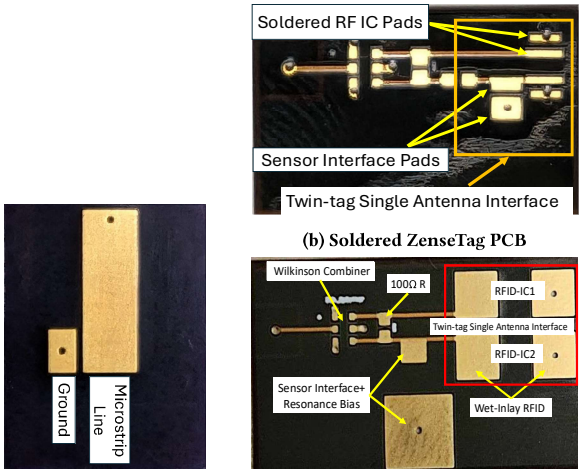

(b) Soldered ZenseTag PCB

(a) Impedance profile PCB **(c) Wet-Inlay ZenseTag PCB**

Figure 11: Different PCBs used in ZenseTag. (a) Simple FR-4 PCB used for sensor impedance profiling. (b),(c) Show the flexible PCs used for the two versions of ZenseTag

4.3 GUI for real-time sensor readout

In order to achieve a real time readout of these sensors using ZenseTag, we developed a Graphical User Interface (GUI) in Python using the SLLURP library [37]. The GUI helps us collect, process and display the processed data in real time as the sensor is being used. SLLURP library [37] allows us to collect data from a commercial Impinj reader in a cyclic fashion, scanning through 50 channels, with 200ms dwell time per channel, resulting in an average data collection rate of 35Hz. First we process raw phase data streaming from the reader by unwrapping it and addressing the π shifts in phase introduced by the channel hopping. In order to correct for the timing discrepancy between the two tag sequences, we compute a moving average over 3 seconds for each time sequence. We average a predetermined number of data points and subsequently calculate the difference between the moving averages of the two sequences.

5 Evaluation

A key contribution of ZenseTag is interfacing commercial sensors to a passive wireless platform with a form factor similar to RFID stickers, using flexible PCBs. We evaluate ZenseTag with three commercial sensors: (1) Soil Moisture Sensor, (2) Force-Sensitive Resistor, and (3) Photodiode. Additionally, we motivate practical case studies to demonstrate on the robustness of ZenseTag's sensor readout. We will first evaluate ZenseTag with a COTS capacitive soil moisture sensor.

5.1 Measuring Soil Moisture using COTS Capacitive Soil Moisture Sensor

To set up this evaluation, we will profile the sensor impedance and then interface it with ZenseTag's flexible PCB using the previously described procedure. **Interfacing Process:** In order to utilize the impedance change of the sensor in a **Direct-to-RF** fashion, we need to interface directly with the bare sensor without any attached electronics that come with it. To do this,the COTS sensor is stripped off of its digital interface (555 timer+bias), and soldered to the impedance profiling PCB using copper wires. The measurement yields a capacitance of 2.2pF and a large equivalent series resistance (ESR) of 37Ω for the sensor. Next the tag is assembled in the optimal shunt topology, and then add a 2.7pF capacitance to tune the resonance and impedance match the commercial soil moisture sensor at RFID frequency. Using the assembled ZenseTag interfaced soil moisture sensor we conduct benchmark evaluations and demonstrate well-motivated practical use-cases.

5.1.1 Benchmarks: **Enhanced Phase Response** To demonstrate the importance of impedance profiling and resonance frequency tuning, we conducted a readout by immersing the sensor in water (100% moisture).We conducted both wired (VNA) and wireless (RFID reader) measurements to observe the sensor's phase change between air and water. After impedance profiling and resonance tuning, the phase change shown by the sensor increased to 15^o compared to $< 1^o$ without, or a **15x improvement** as shown in Fig. 14. We also show two videos to capture this evaluation: **here** [78] and **here** [79].

Power Consumption:

To quantify power consumption in reading COTS sensors (independent of the energy expended on the ADC), we found the interface circuit ($Capacitance \rightarrow AnalogVoltage$) consumes 18mW. In contrast, ZenseTag only measures impedance changes, minimizing power loss to parasitic resistance and mismatch.

5.1.2 Case Study 1: Potted Soil- Moisture Classification For the first use case, we use potted soil in a container and evaluate ZenseTag's ability to classify between Dry, Moist, Saturated Soil moisture. The sensor is placed fully immersed in soil as shown in Fig. 15.

Given the transient, localized and non-deterministic nature of soil moisture, we prepared three different samples: **DRY** when moisture value is <20%, **MOIST** when moisture levels are between 20% and 70% and **SATURATED**, when the moisture level >70%. The precise ground-truth moisture value is obtained by connecting the same sensor to an Arduino and reading it digitally. Simultaneously our data collection software reads and decodes the differential phase. We also conducted measurements over several data points

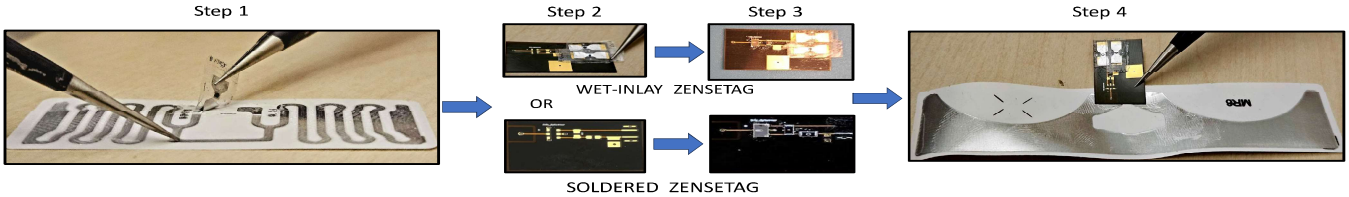

Figure 12: Assembly of flexible and COTS friendly ZenseTag. Step 1: Peel sticker-IC off of RFID tags. Step 2: Attach the ICs to flexible ZenseTag PCB. Step 3: Solder Power Divider and 100Ω resistor. Step 4: Attach PCB to a flexible RFID antenna

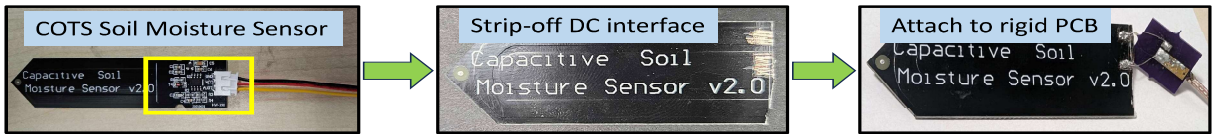

Figure 13: Interfacing a commercial soil moisture sensor:- Step 1: Strip off. Step 2: Small contact pads are etched out to expose copper Step 3: Solder these small leads to rigid impedance profiling PCB.

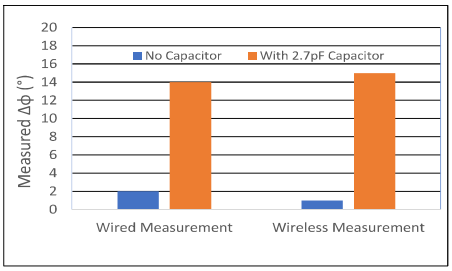

Figure 14: Wired and wireless evaluation of soil moisture interfaced ZenseTag immersed in water, with and without sensor impedance-resonance tuning.

and verified the reliability and repeatability of these readings over a long duration. The video demonstrating our experiment can be **viewed here** [2]. Using the ground truth data obtained from Sensor+Arduino, and the wireless data obtained from samples,we are able to reliably classify between the 3 different moisture levels, even when the sensor is re-inserted in different soil samples prepared independently. The generated confusion matrix (Figs. 15c and 15d.) shows an accuracy **93%**

5.1.3 Case Study 2: Outdoor soil moisture sensing with multiple sensors : We test the sensor in an outdoor environment, by deploying multiple sensors in a patch of soil. In this study, we deployed three ZenseTags equipped with soil moisture sensors into a patch of land as shown in Fig. 15b. We show through this case study that soil moisture is indeed a very localized phenomenon and hence sparse deployments of these sensors cannot capture true moisture in a localized fashion. The measurement is demonstrated in a **recorded video** [80]. The video showcasing the experimental setup can also be found **here** [81].

ZenseTag's ability to measure soil moisture in a granular, localized fashion and its low cost can enable large deployments of such sensors in agricultural farms without the toxic contamination of batteries, or the hassle of laying power cables.

5.2 Measuring Force using COTS FSR

We will now evaluate ZenseTag interfaced with a commercial Force Sensitive Resistor (FSR). We follow a similar interfacing procedure as with soil moisture sensor, except choosing an FSR variant with short leads, to avoid unwanted series resistance.

5.2.1 Interfacing Process: Impedance profiling of a commercial FSR reveals that it (Fig. 4), behaves like a 37nH inductor. We identify and tune its resonance frequency (from 1GHz to 830MHz) using a 1pF capacitor, and connect the FSR in a shunt configuration. as shown in Fig. 16. Using this FSR interfaced ZenseTag, we benchmark its baseline performance.

5.2.2 Benchmarks: Measuring known weights We measure different known weights ranging from 10g to 50g by placing them on the FSR sensor and measuring the differential phase. The results are shown in Fig. 16. From the figure, it is evident that for a **50g change in the load**, ZenseTag is able to produce a phase change of about **30 degrees**, repeatable across multiple trials. Further, we also show that this differential phase can be measured in real time as we press on the sensor several times with our finger. We recorded a **demo video** of the same [1].

5.2.3 Benchmark: Quantifying multipath resilience: A key hurdle under dynamic channel conditions is the corruption of differential phase by multipath, so as a baseline, we must extract uncorrupted phase information even with people and objects moving around the sensor. Prior methods to remedy multipath effects in RFID assisted sensing[31, 32, 35] have used the concept of dual-tags or colocated tags. As detailed in Sec. 2,. 3 we assert that using a compact Wilkinson power combiner is the correct way to remedy multipath effects. In order to evaluate the resilience of ZenseTag sensing platform to dynamic changes in the wireless channel, we conduct an evaluation by keeping the reader and ZenseTag colocated tags fixed as people walk around in Fig. 17. We then compute the phase difference $\Delta\phi$ measured between both the tags, which in this case have no sensor attached. We compare our approach to the other differential approach of co-locating tags. Notably, the median phase difference for ZenseTag is a fixed offset of approx 4° between the two tags which is a **10x better** improvement over co-located tag approach (with phase error $> 40^\circ$)

5.2.4 Case Study: Measuring Human stepping force: Having validated the resilience of ZenseTag to movements around the platform, we evaluate the real-time response of a FSR interfaced ZenseTag, under human stepping impact shown in Fig. 17. We measure the differential phase as a human steps on and off the stepper. To prove the

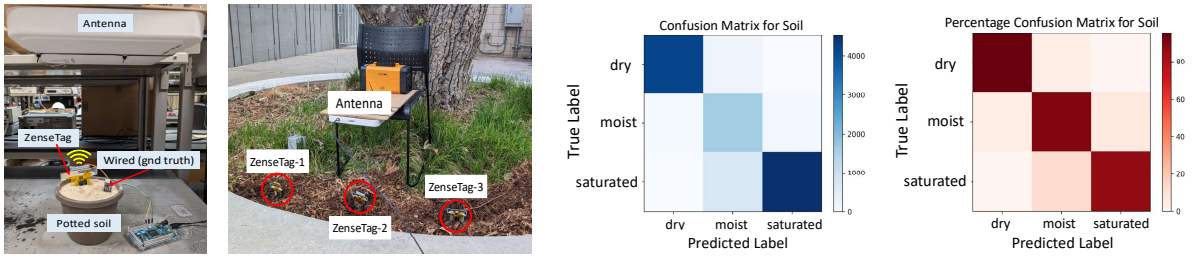

(a) Indoor soil setup (b) Outdoor soil moisture setup (c) Confusion Matrix: All data (d) Confusion Matrix : Accuracy(%)

Figure 15: Wireless sensing of soil moisture using Diff-Z-Tag. We achieve > 93% accuracy across all three moisture levels

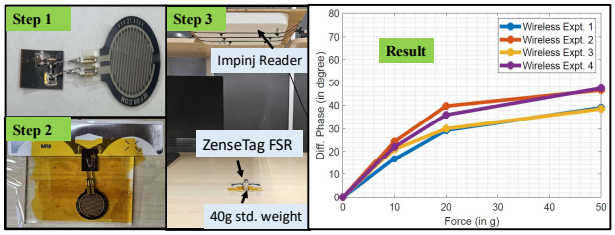

Figure 16: Force sensitive resistor evaluations

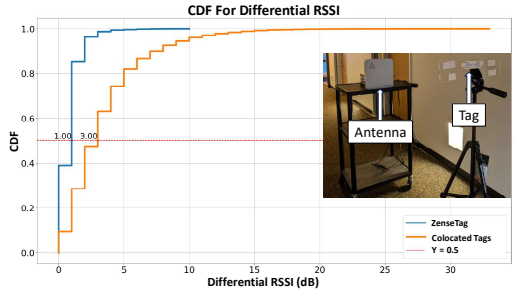

(a) CDF for Differential RSSI. (Inset:Baseline evaluation Setup)

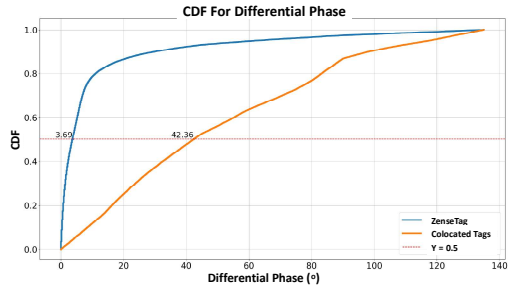

(b) CDF for Differential Phase

Figure 17: Resilience of ZenseTag to multipath in a dynamic channel. We compare the differential analog modulation in ZenseTag with two co-located tags approach. (inset): Tag-Reader setup.

real-time operation of this sensor, we recorded a **demo video** [82]. Differential phase changes repeatably between the same values (accounting for the imperfectness of human stepping) over multiple steps. This case study can motivate interesting applications involving humans playing musical instruments such as piano or drums using a battery-free touch-pad. Furthermore FSR-interfaced ZenseTag system can enablenovel healthcare applications by quantitatively capturing human contact dynamics, such as stepping force during athletic activity. In sports analytics, this can enable wireless and battery-free performance assessment. By measuring precise human contact during stepping exercises, coaches and trainers can gain valuable insights into athletes' efficiency, technique, and biomechanics, informing targeted training regimes, aiding injury prevention, and optimizing performance.

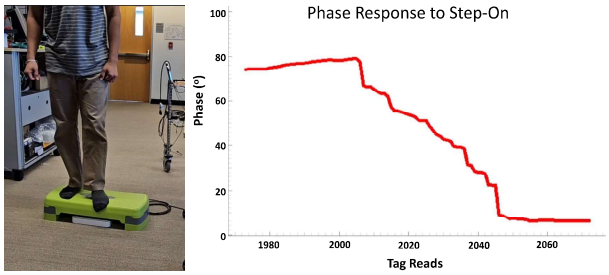

(a) Stepped On (b) Phase Response: Step-On

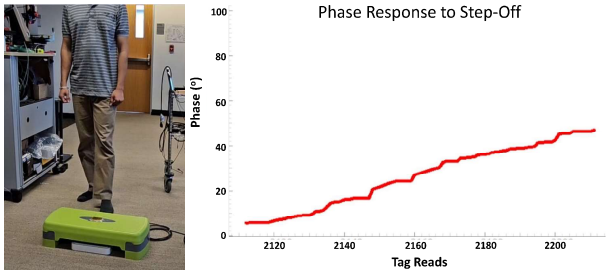

(c) Stepped Off (d) Phase Response: Step-Off

Figure 18: Stepping Exercise using ZenseTag

5.3 Measuring LUX using COTS Photodiode

Light intensity in lux, often measured using photodiodes, is crucial for automating indoor lighting [83, 84], garages [85], and environments with sensitive fauna [86]. Photodiodes are also used in agriculture [87], spectroscopy [88], and industrial automation [89] as color classifiers. Motivated by these applications, we built a photodiode-interfaced ZenseTag and will evaluate its performance as a lux meter and demonstrate a wavelength classifier use-case.

Interfacing Process: Following the procedure in Sec. 3, the impedance of a photodiode was profiled at RF. As shown in Fig. 20 - step 1, at 915MHz, the photodiode exhibits a capacitance of 0.8 pF, offering optimal phase sensitivity in a series configuration. Given that photodiodes are junction devices with low resistance, it behaves almost as an ideal capacitor at RF, without a resonance frequency near the RFID band. Based on the measured impedance profile ZenseTag lux sensor was designed with the photodiode in series, and the experiment is setup as shown in Fig. 20.

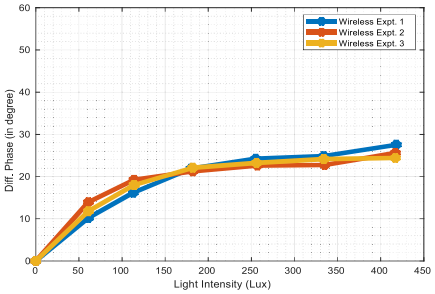

(a) Diff phase vs lux for yellow light.

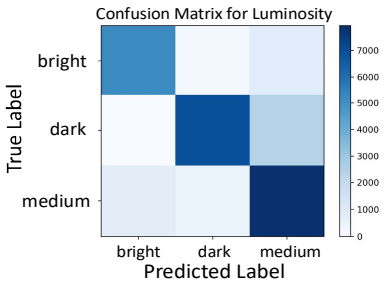

(b) Confusion matrix for all readings

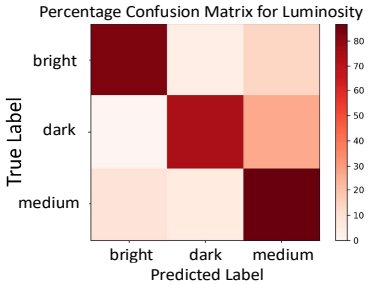

(c) Confusion matrix for ratio of readings

Figure 19: ZenseTag Light sensor wireless results

5.3.1 Benchmark: Measuring Light Intensity using Photodiode Using the setup, we collected differential phase values for varying lux intensities till 400 lux as shown in Fig: 19a. Using three data campaigns conducted at different times, we observe that the phase values are consistent. The sensor response saturates after a lux value of 400. This measurement was taken exposing the sensor to yellow light of varying lux intensity. To ensure minor lux fluctuations are measured, we conducted the measurements in a dark room. Additionally to demonstrate the sensor's repeatability and reliability, measurements were taken over a long duration at three different lux levels: **BRIGHT** (400 lux), **MEDIUM** (180 lux), and **DARK** (0 lux). As shown in Figs. 19b & 19c, we can classify bright and medium with accuracy around **95%**, while dark can be classified with **80%** accuracy.

Live Demo of real-time light intensity sensing: To demonstrate real-time light intensity sensing, we recorded a demo video where the photodiode interfaced ZenseTag was alternately exposed to room light and darkness, showing repeatable performance. The video showing the demonstration can be **viewed here** [3].

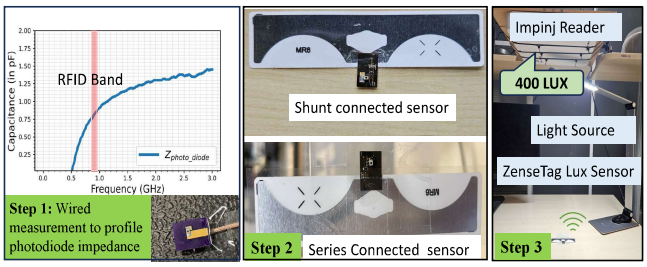

Figure 20: Measuring Lux with ZenseTag. Step 1: Perform impedance profiling of photodiode. Step 2: Connect the photodiode to ZenseTag in the correct topology. Step 3: Setup wireless Lux measurement

5.3.2 Case study: Classifying Colors An interesting observation is that the COTS photodiode used here shows a peak sensitivity to Orange light (λ= 600nm) which is a warm tone. In this case-study we demonstrate photodiode interfaced ZenseTag based wavelength classifier. We evaluated the sensor tag, using lights of three wavelengths - Red, Yellow and Blue. The experiment was carried out in a dark room as shown in Fig. 21a and the differential phase was measured for the ZenseTag light sensor. From the plot in Fig. 21b, we notice a clear monotonic relationship between differential phase and wavelength. Despite lacking high granularity photodiode ZenseTag is still able to reliably classify R-Y-B colours. We envision these sensors in industrial color classifiers for various applications, such as monitoring water quality via spectral signatures, ensuring manufactured goods conform to color standards, and facilitating color-based sorting systems in warehouses.

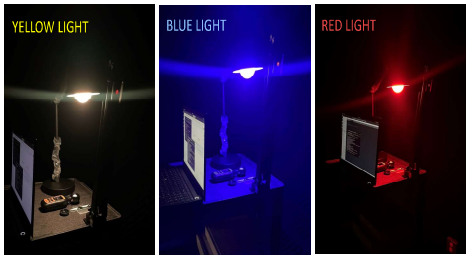

(a) Light Wavelength classification using ZenseTag

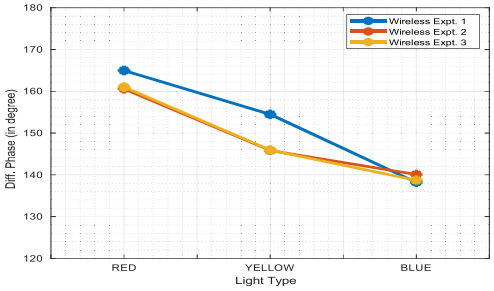

(b) Differential Phase response of ZenseTag for different wavelengths

Figure 21: ZenseTag Setup for wavelength classifier

6 Limitations and Future Work

6.1 Reader cost and size

An obvious challenge with RFID assisted analog sensing is the necessity of a sizeable, non-portable and expensive reader that can perform the communicate with the tags and decode sensor data. However there have been several hand-held and wrist-worn RFID readers that are both affordable and portable [28–30]. We envision that ZenseTag will enable compact sensing tags to become commonplace with increased adoption of such RFID readers.

6.2 Range of operation

RFID tags have range limitations as they depend entirely on harvested energy [90–93]. With the existing prototype, ZenseTag's the worst case readout range is about 50cm depending on the interfaced sensor. While this is lower than the previously reported 1m readout range for a customized designed force-sensor RFID interface [94]

and COTS sensor interface[35], for many of the applications envisioned here the range is sufficient, especially with the availability of newer more portable RFID readers [28, 30, 95].

The loss in range can be accounted to the additional 3 dB loss because of Wilkinson divider, and its impedance mismatch with the RFID tag antenna. This range can be augmented using inductor and capacitor based matching networks as shown in Fig. 22. In order to quantify this range loss, we measured the matched tag with a comparable commercial tag, whose antenna we used. As shown in Fig. 23, we can operate ZenseTag upto 1.25 m range compared to commercial tag. However, a notable point is that, for a commercial RFID tag to be used as a sensor, **prior works occupy 2x the form-factor** of ZenseTag as they need an additional "reference" tag[31, 32, 35, 52] to function. Given this, if the antenna in our design (which takes up the most space relative to the PCB) is increased by more than 2x, its efficiency—and consequently the operating range—will improve significantly [96–98]. The range degradation of ZenseTag compared to commercial tags cannot be fully assessed without considering the form factor. We recommend future research on improved digital twin simulations of the RFID reader-antenna-tag system for holistic analysis and potential solutions[99].

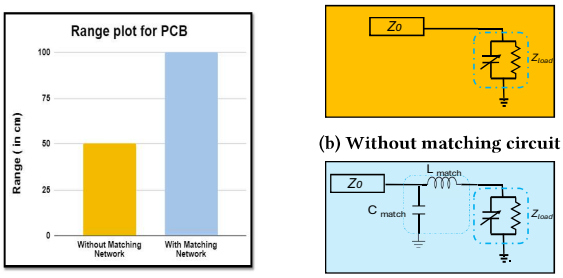

(a) Enhanced range with matching (b) Without matching circuit (c) With matching circuit

Figure 22: Improved sensing range with passive matching circuits

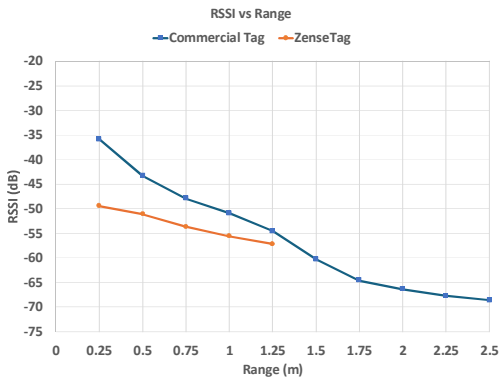

Figure 23: Range degradation due to power divider in ZenseTag compared to a commercial tag. Note that for reliable differential sensing, prior approaches need at least 2X the form factor of ZenseTag.

6.3 Granularity of Sensor Operation

We acknowledge that our work shows a somewhat coarse-level sensing especially for the photodiode tag. This is primarily constrained by the sensitivity (peak at λ=600nm) and performance of the diode itself in response office light. However a different photodiode that has better response under white light could improve the granularity of sensing.

6.4 Robustness to Metal Blockage

In our experiments, the RFID reader and the sensor interface do not assume a metal blocker in between. If there is a metal blocker, the RFID readout will be difficult since there will be no direct path. This limits certain applications, since ideally photodiode backed ZenseTag sensor can be used for parking spot detection in garages, however this will assume a car blocking the photodiode, and hence as of now these applications are not possible. However, further investigation into RFID readouts with metal blockages can potentially alleviate this problem in the future.

6.5 Interfacing Non-Impedance Sensors

The core underlying principle behind the working of ZenseTag is to exploit the impedance change produced by a sensor in response to a stimulus. But its not mandatory that all available sensor produce this effect for us to read it wirelessly. For example, there are gas-sensors [100], that work on a different principle, they have an arc-reactor, that selectively combusts a few gases internal to it. Hence, these sensors are active by default and consume much higher power. Additional examples ionizing radiation sensors[101],piezoelectric structural health monitors etc[102] Although there is ongoing research even here in the sensing community to discover lower power alternatives. Such sensor interfaces with natively active sensors are not possible today with ZenseTag.

6.6 Challenges with Wet-Inlays

The wet-inlay version of ZenseTag is fabricated using the procedure described in Sec. 4 which involves heating the PCB solder components such as Wilkinson Power Combiner and a 100Ω resistor. This tends to heat-related deformation of the PCB which tends to bend it slightly. Consequently, sticking the wet-inlay RFID tags to this PCB is very challenging and requires a significant amount of effort. In the future, this could be addressed by making the entire PCB and assembly through additive manufacturing process such that no heating would be required.

7 Conclusion

In this work, we have presented ZenseTag, a compact, battery-free, wireless sensing platform that can interface commercially available sensors to inexpensive, flexible commercial RFID stickers. Through innovative approaches such as direct-RF interface, sensor resonance tuning and twin-tag-single-antenna interface, ZenseTag achieves superior reliability and accuracy in differential analog sensing of stimuli such as soil moisture, light intensity and contact forces.

8 Acknowledgements

We sincerely thank the anonymous reviewers and the shepherd for their valuable feedback. This work was supported in part by the NSF under the grant number:EFMA-1935329.

References

[1] Force diff-z-tag: Demonstration for a force sensor modulated diff-z-tag. https://www.youtube.com/watch?v=ToExp731PGk, 2024.
[2] Moist diff-z-tag: Demonstration for a soil moisture sensor modulated diff-z-tag. https://www.youtube.com/watch?v=CDn5hxnWvCo, 2024.

[3] Lite diff-z-tag: Demonstration for a photo sensor modulated diff-z-tag. https://www.youtube.com/watch?v=4Gx3-WtXr2U, 2024.

[4] Agrim Gupta, Daegue Park, Shayaun Bashar, Cedric Girerd, Nagarjun Bhat, Siddhi Mundhra, Tania K. Morimoto, and Dinesh Bharadia. Forcesticker: Wireless, batteryless, thin & flexible force sensors. *Proc. ACM Interact. Mob. Wearable Ubiquitous Technol.*, 7(1), mar 2023.

[5] Zhizhang Hu, Amirmohammad Radmehr, Yue Zhang, Shijia Pan, and Phuc Nguyen. Ioteeth: Intra-oral teeth sensing system for dental occlusal diseases recognition. *Proc. ACM Interact. Mob. Wearable Ubiquitous Technol.*, 8(1), mar 2024.

[6] Clementine M. Boutry, Levent Beker, Yukitoshi Kaizawa, Christopher Vassos, Helen Tran, Allison C. Hinckley, Raphael Pfattner, Simiao Niu, Junheng Li, Jean Claverie, Zhen Wang, James Chang, Paige M. Fox, and Zhenan Bao. Biodegradable and flexible arterial-pulse sensor for the wireless monitoring of blood flow. *Nature Biomedical Engineering*, 3(1):47–57, January 2019.

[7] Tina Naghdi, Hamed Golmohammadi, Hossein Yousefi, Mohammad Hosseinifard, Uliana Kostiv, Daniel Horák, and Arben Merkoçi. Chitin nanofiber paper toward optical (bio)sensing applications. *ACS Applied Materials and Interfaces*, 12(13):15538–15552, March 2020.

[8] Namgyeong Jo, Bongjun Kim, Sun-Mi Lee, Jeseung Oh, In Ho Park, Kook Jin Lim, Jeon-Soo Shin, and Kyung-Hwa Yoo. Aptamer-functionalized capacitance sensors for real-time monitoring of bacterial growth and antibiotic susceptibility. *Biosensors and Bioelectronics*, 102:164–170, April 2018.

[9] Jae K. Jung and Ji H. Lee. High-performance hydrogen gas sensor system based on transparent coaxial cylinder capacitive electrodes and a volumetric analysis technique. *Scientific Reports*, 14(1), January 2024.

[10] Jayavardhana Gubbi, Rajkumar Buyya, Slaven Marusic, and Marimuthu Palaniswami. Internet of things (iot): A vision, architectural elements, and future directions. *Future Generation Computer Systems*, 29(7):1645–1660, 2013. Including Special sections: Cyber-enabled Distributed Computing for Ubiquitous Cloud and Network Services Cloud Computing and Scientific Applications — Big Data, Scalable Analytics, and Beyond.

[11] Joshua R. Smith, Alanson P. Sample, Pauline S. Powledge, Sumit Roy, and Alexander Mamishev. A wirelessly-powered platform for sensing and computation. In Paul Dourish and Adrian Friday, editors, *UbiComp 2006: Ubiquitous Computing*, pages 495–506, Berlin, Heidelberg, 2006. Springer Berlin Heidelberg.

[12] Rohan Menon, Rohit Gujarathi, Ali Saffari, and Joshua R. Smith. Wireless identification and sensing platform version 6.0. In *Proceedings of the 20th ACM Conference on Embedded Networked Sensor Systems*, SenSys '22, page 899–905, New York, NY, USA, 2023. Association for Computing Machinery.

[13] *Wirelessly Powered Sensor Networks and Computational RFID*. Springer New York, 2013.

[14] sensor readout power consumption. https://www.analog.com/en/resources/analog-dialogue/articles/optimizing-energy-use-in-advanced-sensors.html, 2021.

[15] Caleb D Johnson, Adam S Tenforde, Jereme Outerleys, Julia Reilly, and Irene S Davis. Impact-related ground reaction forces are more strongly associated with some running injuries than others. *Am. J. Sports Med.*, 48(12):3072–3080, October 2020.

[16] Tuo Yu, Haiming Jin, and Klara Nahrstedt. Shoesloc: In-shoe force sensor-based indoor walking path tracking. *Proc. ACM Interact. Mob. Wearable Ubiquitous Technol.*, 3(1), mar 2019.

[17] Brian Horsak, Djordje Slijepcevic, Anna-Maria Raberger, Caterine Schwab, Marianne Worisch, and Matthias Zeppelzauer. Gaitrec, a large-scale ground reaction force dataset of healthy and impaired gait. *Scientific Data*, 7(1), May 2020.

[18] Unang Sunarya, Yuli Sun Hariyani, Taeheum Cho, Jongryun Roh, Joonho Hyeong, Illsoo Sohn, Sayup Kim, and Cheolsoo Park. Feature analysis of smart shoe sensors for classification of gait patterns. *Sensors*, 20(21):6253, November 2020.

[19] Shoe insole force sensor. https://moticon.com/opengo/sensor-insoles, 2020.

[20] Nivedita Arora, Vikram Iyer, Hyunjoo Oh, Gregory D. Abowd, and Josiah D. Hester. Circularity in energy harvesting computational "things". In *Proceedings of the 20th ACM Conference on Embedded Networked Sensor Systems*, SenSys '22, page 931–933, New York, NY, USA, 2023. Association for Computing Machinery.

[21] Ravi Manne and Sneha Chowdary Kantheti. Green iot towards environmentally friendly, sustainable and revolutionized farming. *Green Internet of Things and Machine Learning: Towards a Smart Sustainable World*, pages 113–139, 2021.

[22] Prashobh Karunakaran, Shanthi Karunakaran, Mohammad Shahril Osman, Sreeja Haridas, Prashanth Karunakaran, and Arjun Karunakaran. Farming with the utilization of iot. *Global Journal of Engineering and Technology Advances*, 16(2):124–134, 2023.

[23] Xin Na, Xiuzhen Guo, Zihao Yu, Jia Zhang, Yuan He, and Yunhao Liu. Leggiero: Analog wifi backscatter with payload transparency. In *Proceedings of the 21st Annual International Conference on Mobile Systems, Applications and Services*, MobiSys '23, page 436–449, New York, NY, USA, 2023. Association for Computing Machinery.

[24] Elahe Soltanaghaei, Adwait Dongare, Akarsh Prabhakara, Swarun Kumar, Anthony Rowe, and Kamin Whitehouse. Tagfi: Locating ultra-low power wifi tags using unmodified wifi infrastructure. *Proc. ACM Interact. Mob. Wearable Ubiquitous Technol.*, 5(1), March 2021.

[25] Joshua F. Ensworth and Matthew S. Reynolds. Ble-backscatter: Ultralow-power iot nodes compatible with bluetooth 4.0 low energy (ble) smartphones and tablets. *IEEE Transactions on Microwave Theory and Techniques*, 65(9):3360–3368, 2017.

[26] Haotian Jiang, Jiacheng Zhang, Xiuzhen Guo, and Yuan He. Sense me on the ride: Accurate mobile sensing over a lora backscatter channel. In *Proceedings of the 19th ACM Conference on Embedded Networked Sensor Systems*, SenSys '21, page 125–137, New York, NY, USA, 2021. Association for Computing Machinery.

[27] Farzan Dehbashi, Ali Abedi, Tim Brecht, and Omid Abari. Verification: can wifi backscatter replace rfid? In *Proceedings of the 27th Annual International Conference on Mobile Computing and Networking*, MobiCom '21, page 97–107, New York, NY, USA, 2021. Association for Computing Machinery.

[28] Rfid wristbands. https://www.yarongtech.com/collections/rfid-wristbands, 2021.

[29] Rfid wristbands. https://www.zebra.com/us/en/products/spec-sheets/rfid/rfid-handhelds/rfd8500.html, 2021.

[30] Laura Dodds, Isaac Perper, Aline Eid, and Fadel Adib. *A Handheld Fine-Grained RFID Localization System with Complex-Controlled Polarization*. Association for Computing Machinery, New York, NY, USA, 2023.

[31] Wei Sun and Kannan Srinivasan. Healthy diapering with passive rfids for diaper wetness sensing and urine ph identification. MobiSys '21, page 188–201, New York, NY, USA, 2021. Association for Computing Machinery.

[32] Ju Wang, Liqiong Chang, Shourya Aggarwal, Omid Abari, and Srinivasan Keshav. Soil moisture sensing with commodity rfid systems. In *Proceedings of the 18th International Conference on Mobile Systems, Applications, and Services*, MobiSys '20, page 273–285, New York, NY, USA, 2020. Association for Computing Machinery.

[33] Xingyu Chen, Jia Liu, Fu Xiao, Shigang Chen, and Lijun Chen. Thermotag: item-level temperature sensing with a passive rfid tag. In *Proceedings of the 19th Annual International Conference on Mobile Systems, Applications, and Services*, pages 163–174, 2021.

[34] John Nolan, Kun Qian, and Xinyu Zhang. Keystub: A passive rfid-based keypad interface using resonant stubs. *Proc. ACM Interact. Mob. Wearable Ubiquitous Technol.*, 7(4), jan 2024.

[35] Ju Wang, Omid Abari, and Srinivasan Keshav. Challenge: Rfid hacking for fun and profit. In *Proceedings of the 24th Annual International Conference on Mobile Computing and Networking*, MobiCom '18, page 461–470, New York, NY, USA, 2018. Association for Computing Machinery.

[36] Unsoo Ha, Junshan Leng, Alaa Khaddaj, and Fadel Adib. Food and liquid sensing in practical environments using rfids. In *Proceedings of the 17th Usenix Conference on Networked Systems Design and Implementation*, NSDI'20, page 1083–1100, USA, 2020. USENIX Association.

[37] ransford. Pure-python client for llrp-based rfid readers. https://github.com/sllurp/sllurp, 2023.

[38] Shoe insole force sensor. https://gikfun.com/products/gikfun-capacitive-soil-moisture-sensor-corrosion-resistant-for-arduino-moisture-detection-garden-watering-diy-pack-of-2pcs, 2020.

[39] Force sensitive resistor. https://www.interlinkelectronics.com/fsr-400-series, 2021.

[40] Osram. ble-iot. https://www.mouser.com/datasheet/2/588/prd_pim_datasheet_28478303_EN_pdf-3392393.pdf, 2021.

[41] Michael Buettner, Richa Prasad, Alanson Sample, Daniel Yeager, Ben Greenstein, Joshua R Smith, and David Wetherall. Rfid sensor networks with the intel wisp. In *Proceedings of the 6th ACM conference on Embedded network sensor systems*, pages 393–394, 2008.

[42] Saman Naderiparizi, Zerina Kapetanovic, and Joshua R. Smith. Wispcam: An rf-powered smart camera for machine vision applications. In *Proceedings of the 4th International Workshop on Energy Harvesting and Energy-Neutral Sensing Systems*, ENSsys '16, page 19–22, New York, NY, USA, 2016. Association for Computing Machinery.

[43] R. Min, M. Bhardwaj, Seong-Hwan Cho, E. Shih, A. Sinha, A. Wang, and A. Chandrakasan. Low-power wireless sensor networks. In *VLSI Design 2001. Fourteenth International Conference on VLSI Design*, pages 205–210, 2001.

[44] Li Huang, Maryam Ashouei, Firat Yazicioglu, Julien Penders, Ruud Vullers, Guido Dolmans, Patrick Merken, Jos Huisken, Harmke de Groot, Chris Van Hoof, et al. Ultra-low power sensor design for wireless body area networks: Challenges, potential solutions, and applications. *International Journal of Digital Content Technology and its Applications*, 3(3):136–148, 2009.

[45] Rishi Shukla, Neev Kiran, Rui Wang, Jeremy Gummeson, and Sunghoon Ivan Lee. Skinnypower: enabling batteryless wearable sensors via intra-body power transfer. In *Proceedings of the 17th Conference on Embedded Networked Sensor Systems*, SenSys '19, page 68–82, New York, NY, USA, 2019. Association for Computing Machinery.

[46] Andreas Soleiman and Ambuj Varshney. Backscatter-enabled polymorphic light sensors (demo). In *Proceedings of the 17th Annual International Conference on Mobile Systems, Applications, and Services*, MobiSys '19, page 683–684, New York, NY, USA, 2019. Association for Computing Machinery.

[47] Xiaozhou Lü, Yebo Tao, Kai Xie, Songlin Wang, Xiaoping Li, Weimin Bao, and Renjie Chen. A photodiode based miniature sun sensor. *Measurement Science and Technology*, 28(5):055104, April 2017.

[48] Vaishnavi Ranganathan, Sidhant Gupta, Jonathan Lester, Joshua R Smith, and Desney Tan. Rf bandaid: A fully-analog and passive wireless interface for wearable sensors. *Proceedings of the ACM on Interactive, Mobile, Wearable and Ubiquitous Technologies*, 2(2):1–21, 2018.

[49] Nivedita Arora, Ali Mirzazadeh, Injoo Moon, Charles Ramey, Yuhui Zhao, Daniela C. Rodriguez, Gregory D. Abowd, and Thad Starner. Mars: Nanopower battery-free wireless interfaces for touch, swipe and speech input. In *The 34th Annual ACM Symposium on User Interface Software and Technology*, UIST '21, page 1305–1325, New York, NY, USA, 2021. Association for Computing Machinery.

[50] Laiba Shahid, Humayun Shahid, Muhammad Ali Riaz, Syeda Iffat Naqvi, Mansoor Shaukat Khan, Yasar Amin, Jonathan Loo, et al. Chipless rfid tag for touch event sensing and localization. *IEEE Access*, 8:502–513, 2019.

[51] Federica Naccarata, Giulio Maria Bianco, and Gaetano Marrocco. Sensing performance of multi-channel rfid-based finger augmentation devices for tactile internet. *IEEE Journal of Radio Frequency Identification*, 6:209–217, 2022.

[52] Jingxian Wang, Chengfeng Pan, Haojian Jin, Vaibhav Singh, Yash Jain, Jason I. Hong, Carmel Majidi, and Swarun Kumar. Rfid tattoo: A wireless platform for speech recognition. *Proc. ACM Interact. Mob. Wearable Ubiquitous Technol.*, 3(4), sep 2020.

[53] Hanchuan Li, Eric Brockmeyer, Elizabeth J Carter, Josh Fromm, Scott E Hudson, Shwetak N Patel, and Alanson Sample. Paperid: A technique for drawing functional battery-free wireless interfaces on paper. In *Proceedings of the 2016 CHI Conference on Human Factors in Computing Systems*, pages 5885–5896, 2016.

[54] Hanchuan Li, Can Ye, and Alanson P Sample. Idsense: A human object interaction detection system based on passive uhf rfid. In *Proceedings of the 33rd Annual ACM Conference on Human Factors in Computing Systems*, pages 2555–2564, 2015.

[55] Jun Zhang, Gui Yun Tian, Adi MJ Marindra, Ali Imam Sunny, and Ao Bo Zhao. A review of passive rfid tag antenna-based sensors and systems for structural health monitoring applications. *Sensors*, 17(2):265, 2017.

[56] Bhawana Chhaglani, Camellia Zakaria, Richard Peltier, Jeremy Gummeson, and Prashant Shenoy. Aerosense: Sensing aerosol emissions from indoor human activities. *Proc. ACM Interact. Mob. Wearable Ubiquitous Technol.*, 8(2), may 2024.

[57] Tuan Dang, Trung Tran, Khang Nguyen, Tien Pham, Nhat Pham, Tam Vu, and Phuc Nguyen. Iotree: a battery-free wearable system with biocompatible sensors for continuous tree health monitoring. In *Proceedings of the 28th Annual International Conference on Mobile Computing And Networking*, MobiCom '22, page 352–366, New York, NY, USA, 2022. Association for Computing Machinery.

[58] Ge Wang, Lubing Han, Yuance Chang, Yuting Shi, Chen Qian, Cong Zhao, Han Ding, Wei Xi, Cui Zhao, and Jizhong Zhao. Cross-technology communication between visible light and battery-free rfids. *Proceedings of the ACM on Interactive, Mobile, Wearable and Ubiquitous Technologies*, 7(3):1–20, 2023.

[59] Bill Yen, Laura Jaliff, Louis Gutierrez, Philothei Sahinidis, Sadie Bernstein, John Madden, Stephen Taylor, Colleen Josephson, Pat Pannuto, Weitao Shuai, George Wells, Nivedita Arora, and Josiah Hester. Soil-powered computing: The engineer's guide to practical soil microbial fuel cell design. *Proc. ACM Interact. Mob. Wearable Ubiquitous Technol.*, 7(4), January 2024.

[60] Xieyang Xu, Yang Shen, Junrui Yang, Chenren Xu, Guobin Shen, Guojun Chen, and Yunzhe Ni. Passivevlc: Enabling practical visible light backscatter communication for battery-free iot applications. In *Proceedings of the 23rd Annual International Conference on Mobile Computing and Networking*, MobiCom '17, page 180–192, New York, NY, USA, 2017. Association for Computing Machinery.

[61] Jiangtao Li, Angli Liu, Guobin Shen, Liqun Li, Chao Sun, and Feng Zhao. Retro-vlc: Enabling battery-free duplex visible light communication for mobile and iot applications. In *Proceedings of the 16th International Workshop on Mobile Computing Systems and Applications*, HotMobile '15, page 21–26, New York, NY, USA, 2015. Association for Computing Machinery.

[62] Vamsi Talla, Bryce Kellogg, Shyamnath Gollakota, and Joshua R. Smith. Battery-free cellphone. *Proc. ACM Interact. Mob. Wearable Ubiquitous Technol.*, 1(2), June 2017.

[63] Vamsi Talla and Joshua R. Smith. Hybrid analog-digital backscatter: A new approach for battery-free sensing. In *2013 IEEE International Conference on RFID (RFID)*, pages 74–81, 2013.

[64] Brandon Oubre, Spencer Lane, Skylar Holmes, Katherine Boyer, and Sunghoon Ivan Lee. Estimating ground reaction force and center of pressure using low-cost wearable devices. *IEEE Transactions on Biomedical Engineering*, 69(4):1461–1468, 2022.

[65] Melih Ogeday Cicek, Doga Doganay, Mete Batuhan Durukan, Mustafa Caner Gorur, and Husnu Emrah Unalan. Seamless monolithic design for foam based, flexible, parallel plate capacitive sensors. *Advanced materials technologies*, 6(6):2001168, 2021.

[66] Infineon-antenna-aperture-tuning. https://www.infineon.com/cms/en/product/rf/antenna-tuners/, 2019.

[67] Mahmoud Wagih, Alex S. Weddell, and Steve Beeby. Battery-free wireless light-sensing tag based on a long-range dual-port dual-polarized rfid platform. *Sensors*, 22(13), 2022.

[68] Xiaojiao Yang, Bizao Wu, Shixun Wu, Xinxin Liu, W. G. Will Zhao, and Zhili Zhou. Time slot detection-based m-ary tree anticollision identification protocol for rfid tags in the internet of things. *Wirel. Commun. Mob. Comput.*, 2021, January 2021.

[69] Rafael Perazzo Barbosa Mota and Daniel M. Batista. A dynamic frame slotted aloha anti-collision algorithm for the internet of things. In *Proceedings of the 29th Annual ACM Symposium on Applied Computing*, SAC '14, page 686–691, New York, NY, USA, 2014. Association for Computing Machinery.

[70] Keysight. Lcr meter. https://www.keysight.com/us/en/product/E4980A/precision-lcr-meter-20-hz-2-mhz.html, 2021.

[71] Texas Instruments David Wang. Basics of capacitive sensing and applications. https://www.ti.com/lit/an/snoa927a/snoa927a.pdf?ts=1705896122811&ref_url=https%253A%252F%252Fwww.bing.com%252F, 2021.

[72] keysight 5071c vna. https://www.keysight.com/us/en/product/E5071C/e5071c-ena-vector-network-analyzer.html, 2022.

[73] Joel P. Dunsmore. *Handbook of Microwave Component Measurements: with Advanced VNA Techniques*. Wiley, June 2020.

[74] Ansys digital twin. https://www.keysight.com/us/en/products/software/pathwave-design-software/pathwave-advanced-design-system.html.

[75] Ansys digital twin. https://www.ansys.com/products/electronics/ansys-hfss, 2023.

[76] NXP. Sl3s1202 soldered rfid. https://www.digikey.com/en/products/detail/SL3S1202FTB1%2c115, 2021.

[77] NXP. Wet inlay rfid tag. https://www.atlasrfidstore.com/avery-dennison-ad-238u8-uhf-rfid-wet-inlay-nxp-ucode-8/, 2021.

[78] Wired measurement of a soil moisture sensor (biased with a capacitor). https://www.youtube.com/watch?v=fzTxb7nYeoM, 2024.

[79] Wired measurement of soil moisture sensor (without capacitor). https://www.youtube.com/watch?v=MnOtdZxlcu8, 2024.

[80] Moist diff-z-tag: Demonstration of outdoor environment using multiple moist diff-z-tags. https://www.youtube.com/watch?v=7eiO4BO_wTQ, 2024.

[81] Moist diff-z-tag: Experimental setup for demonstrating the use of multiple moist diff-z-tags. https://www.youtube.com/watch?v=yuTeK2nPzGA, 2024.

[82] Force diff-z-tag: Demonstration of a stepping exercise using a force sensor modulated diff-z-tag. https://www.youtube.com/watch?v=spO8E3l9P-U, 2024.

[83] Gianfranco Andia Vera, Shankar D Nawale, Smail Tedjini, and Yvan Duroc. Passive uhf rfid backscattering for indoor lighting control. In *2014 Annual IEEE India Conference (INDICON)*, pages 1–4, 2014.

[84] Daniel Konings, Nathaniel Faulkner, Fakhrul Alam, Edmund M.-K. Lai, and Serge Demidenko. Fieldlight: Device-free indoor human localization using passive visible light positioning and artificial potential fields. *IEEE Sensors Journal*, 20(2):1054–1066, Jan 2020.

[85] G. Aravindh and M. Arun Kumar. An efficient car parking management system using raspberry-pi. In *2020 3rd International Conference on Intelligent Sustainable Systems (ICISS)*, pages 154–158, 2020.

[86] Rachel Yotter and Denise Wilson. A review of photodetectors for sensing light-emitting reporters in biological systems. *Sensors Journal, IEEE*, 3:288 – 303, 07 2003.

[87] Ioan Lita, Daniel Alexandru Visan, Laurentiu Mihai Ionescu, and Alin Gheorghita Mazare. Color-based sorting system for agriculture applications. In *2019 11th International Conference on Electronics, Computers and Artificial Intelligence (ECAI)*, pages 1–4, 2019.

[88] Xue Wu and Kaushik Sengupta. On-chip thz spectroscope exploiting electromagnetic scattering with multi-port antenna. *IEEE Journal of Solid-State Circuits*, 51(12):3049–3062, 2016.

[89] M. Tartagni, E. Franchi, R. Guerrieri, and G. Baccarani. A photodiode cell for applications to position and motion estimation sensors. *IEEE Transactions on Industrial Electronics*, 43(1):200–206, 1996.

[90] Peter Darcy, Prapassara Pupunwiwat, and Bela Stantic. The challenges and issues facing the deployment of rfid technology. *Deploying RFID–challenges, solutions and open. issues. Rijeka: I-Tech Education and. Publishing KG*, pages 1–12, 2011.

[91] Miodrag Bolic, David Simplot-Ryl, and Ivan Stojmenovic. Rfid systems: research trends and challenges. 2010.

[92] Mohamad Katanbaf, Ali Saffari, and Joshua R. Smith. Receiver selectivity limits on bistatic backscatter range. In *2020 IEEE International Conference on RFID (RFID)*, pages 1–8, 2020.

[93] Vamsi Talla, Joshua Smith, and Shyamnath Gollakota. Advances and open problems in backscatter networking. *GetMobile: Mobile Comp. and Comm.*, 24(4):32–38, mar 2021.

[94] Agrim Gupta, Cédric Girerd, Manideep Dunna, Qiming Zhang, Raghav Subbaraman, Tania Morimoto, and Dinesh Bharadia. {WiForce}: Wireless sensing and

localization of contact forces on a space continuum. In *18th USENIX Symposium on Networked Systems Design and Implementation (NSDI 21)*, pages 827–844, 2021.

[95] Zebra. WS50 Android Wearable Computer| Zebra — zebra.com. https://www.zebra.com/us/en/products/mobile-computers/wearable-computers/ws50.html. [Accessed 02-07-2024].

[96] Roger F. Harrington. Effect of antenna size on gain, bandwidth, and efficiency. *Journal of Research of the National Bureau of Standards, Section D: Radio Propagation*, page 1, 1960.

[97] Randy Bancroft. Fundamental Dimension Limits of Antennas. https://people.eecs.berkeley.edu/~culler/AIIT/papers/radio/antenna%20wp_dimension_limits.pdf. [Accessed 30-09-2024].

[98] L. J. Chu. Physical limitations of omni-directional antennas. *Journal of Applied Physics*, 19(12):1163–1175, 1948.

[99] Matthew S Trotter and Gregory D Durgin. Survey of range improvement of commercial rfid tags with power optimized waveforms. In *2010 IEEE International Conference on RFID (IEEE RFID 2010)*, pages 195–202. IEEE, 2010.

[100] Nima Afshar-Mohajer, Christopher Zuidema, Sinan Sousan, Laura Hallett, Marcus Tatum, Ana M. Rule, Geb Thomas, Thomas M. Peters, and Kirsten Koehler. Evaluation of low-cost electro-chemical sensors for environmental monitoring of ozone, nitrogen dioxide, and carbon monoxide. *Journal of Occupational and Environmental Hygiene*, 15(2):87–98, October 2017.

[101] Mirion. Introduction to Radiation Detectors — mirion.com. https://www.mirion.com/discover/knowledge-hub/articles/education/introduction-to-radiation-detectors. [Accessed 30-09-2024].

[102] Min Ju, Zhongshang Dou, Jia-Wang Li, Xuting Qiu, Binglin Shen, Dawei Zhang, Fang-Zhou Yao, Wen Gong, and Ke Wang. Piezoelectric materials and sensors for structural health monitoring: Fundamental aspects, current status, and future perspectives. *Sensors*, 23(1):543, January 2023.